A measurement method for the estimation of the absorption characteristics of finite-sized porous absorbers

Gergely Firtha[1*], Péter Fiala[1]

[1]Department of Networked Systems and Services, Faculty of Electric Engineering,
Budapest University of Technology and Economics, Műegyetem rkp. 3., H-1111 Budapest, Hungary
[*]Corresponding author, e-mail: firtha@hit.bme.hu

Abstract

The estimation of sound fields generated inside enclosures has gained increasing interest in the recent years, both for acoustic design purposes and virtual reality applications. Numerical simulation methods require detailed information on the impedance/absorption characteristics of the enclosing surfaces. The currently available measurement methods are only capable of obtaning the point-like impedance of locally reacting surfaces. We present a new measurement technique to characterize extended reacting absorbing surfaces. The measurement is done by scanning the surface with a PU-probe, and the asborption characteristics are obtained by a Helmholtz-integral based postprocessing step.

Keywords:

absorption measurement; extendedly reactive surfaces, porous absorption, admittance matrix

1. Introduction

The measurement of the absorption properties of acoustic materials is of significant importance in the field of acoustic modeling and acoustic design. The ISO 354:2003 standard [1] provides a reverberation chamber based absorption measurement technique that allows the estimation of the statistical random incident absorption for samples exceeding an area of $10\,\mathrm{m}^2$. As a further measurement approach, the ISO 10534-2:1998 standard [2] outlines the use of an impedance-tube and in-situ (e.g. two microphone free field measurement) methods to derive specific impedance at a given positions on an absorber surface, which subsequently facilitates the calculation of normal incidence absorption coefficients.

All the aforementioned impedance measurement techniques assume that the acoustic behavior of the absorbing surface is determined merely by the point-like specific impedance at the measurement position. This approach, known as the *locally reacting surface* assumption, completely disregards the lateral wave propagation occurring within the absorber material. For certain acoustic structures, such as the surface of a thin layer of porous material, it is indeed feasible to model them as locally reacting surfaces, provided that the material sample is large enough to neglect diffracted waves from the edges and thin enough to ignore lateral wave propagation within the material. To ensure the validity of this assumption, traditional standard impedance measurement techniques require material samples with an area exceeding $1\,\mathrm{m}^2$ [3].

The assumptions of local reaction become inadequate when lateral wave propagation significantly affects the test ma-terial, often leading to absorption coefficients higher than unity [4, 5]. Such materials are commonly known as *non-locally* or *extendedly reacting surfaces* [6]. Examples of extendedly reactive surfaces include simple plate resonators or a layer of small-sized porous absorbing material.

Recently, the current authors proposed a novel measurement method for predicting the absorption properties of planar extendedly reactive surfaces. The underlying physical model relies on the a-priori knowledge of the self- and mutual admittances at positions on the absorber surface, represented by the admittance matrix. This allows for a numerical solution for the acoustic scattering of an arbitrary incident field from which absorption properties can be estimated. The primary challenge of this approach is measuring the surface's admittance matrix. In a previous work [7], the authors investigated the measurement of a plate absorber. In this paper, we explore the application of this methodology to predict the absorption characteristics of a framed porous layer with relatively small spatial extension, relying on an extended two-microphone measurement for acquiring the admittance matrix.

The paper is structured as follows: Section 2 introduces the mathematical-physical model that was used in order to predict the reflected field, scattered from an extended reactive—i.e. elastic—surface, from which the absorption characteristics can be estimated. Section 3 describes the measurement methodology used in order to estimate the surface admittance matrix. Finally, Section 4 presents the estimated absorption characteristics of the porous absorber, followed by a brief summary.
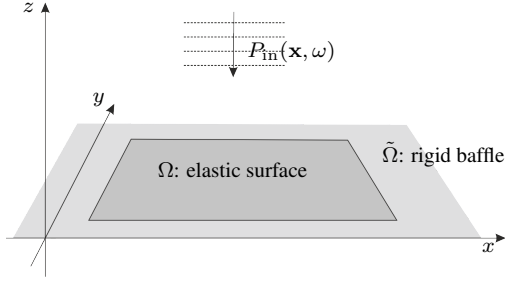
Figure 1: Geometry for scattering from an elastic surface.

2. Methodology

2.1. Physical model for scattering from elastic surfaces

Assume a finite, planar extended reactive (elastic) surface, baffled into an infinite rigid plane at $z = 0$, as depicted in Figure 1 with an exemplary rectangular surface. As a simple example, the surface is the top of a porous material, backed and framed rigidly. We use the symbol Ω to refer to points located on the elastic surface and $\tilde{\Omega}$ to indicate positions on the rigid baffle.

The plane is loaded by the infinite half-space consisting of fluid of density ρ_0 in which the speed of sound is denoted by c. The planar surface is exposed to an arbitrary steady-state incident wave field $P_{\text{in}}(\mathbf{x}, \omega)$, propagating towards the elastic plate and oscillating at an angular frequency ω. As the incident wave is scattered from the surface, three main components can be identified in the resulting total pressure field:

- The incident field $P_{\text{in}}(\mathbf{x}, \omega)$

- A part of the incident field is reflected directly from the surface due to the impedance jump, denoted by $P_{\text{refl}}(\mathbf{x}, \omega)$; and

- A part of the sound energy enters through the surface, causing the motion of the medium below. This vibration re-radiates a sound wave into the positive half space, denoted by $P_{\text{rerad}}(\mathbf{x}, \omega)$.

The latter two components together build the scattered field, denoted by P_{scat}. Our aim is to evaluate the total pressure field, written as

$$P_{\text{tot}}(\mathbf{x}, \omega) = P_{\text{in}}(\mathbf{x}, \omega) + \underbrace{P_{\text{refl}}(\mathbf{x}, \omega) + P_{\text{rerad}}(\mathbf{x}, \omega)}_{P_{\text{scat}}(\mathbf{x}, \omega)}, \tag{1}$$

assuming that the equation of motion of the elastic surface is known. For the sake of brevity we omit noting the dependence on angular frequency.

The boundary conditions can be formulated in the present geometry as follows:

- On the infinite rigid baffle the total velocity is zero, yielding

$$\frac{\partial}{\partial z} P_{\text{in}}(\mathbf{x}) = -\frac{\partial}{\partial z} P_{\text{scat}}(\mathbf{x}) \tag{2}$$

$$P_{\text{in}}(\mathbf{x}) = P_{\text{scat}}(\mathbf{x}), \qquad \mathbf{x} \in \tilde{\Omega} \tag{3}$$

- On the elastic surface it is assumed that the transfer admittance is defined between each point, defined as

$$A(\mathbf{x}) = \int_\Omega Y(\mathbf{x}, \mathbf{x}_0) P(\mathbf{x}_0) \, d\mathbf{x}_0, \tag{4}$$

where $A(\mathbf{x})$ is the normal acceleration of the surface at $\mathbf{x}$, and $P(\mathbf{x}_0)$ is the pressure at $\mathbf{x}_0$. The admittance function, therefore, is defined as the acceleration of the surface, assuming the pressure distribution of a Dirac-delta:

$$Y(\mathbf{x}, \mathbf{x}_0) = A(\mathbf{x}), \quad \text{if} \ \ P(\mathbf{x}) = \delta(\mathbf{x} - \mathbf{x}_0) \tag{5}$$

For the present planar geometry the scattered field can be written in terms of a Rayleigh integral over the elastic surface (inherently exploiting that the rigid baffle does not contribute to the integral) [8, 9], resulting in the expression for the total field at an arbitrary receiver position $\mathbf{x} = [x, \ y, \ z \geq 0]^{\mathrm{T}}$

$$P_{\text{tot}}(\mathbf{x}) = P_{\text{in}}(\mathbf{x}) - 2 \int_\Omega \frac{\partial}{\partial z} P_{\text{scat}}(\mathbf{x}_0) G(\mathbf{x}, \mathbf{x}_0) d\mathbf{x}_0, \tag{6}$$

with the shortened notation $\frac{\partial}{\partial z} P_{\text{scat}}(\mathbf{x}_0) = \frac{\partial}{\partial z} P_{\text{scat}}(\mathbf{x})\big|_{\mathbf{x}=\mathbf{x}_0}$. Here G denotes the 3D Green's function

$$G(\mathbf{x}, \mathbf{x}_0) = \frac{1}{4\pi} \frac{e^{-j\frac{\omega}{c}|\mathbf{x}-\mathbf{x}_0|}}{|\mathbf{x} - \mathbf{x}_0|} \tag{7}$$

describing the field of a point source located at $\mathbf{x}_0$, measured at $\mathbf{x}$.

Expressing $P_{\text{scat}}(\mathbf{x}_0)$ as $P_{\text{tot}}(\mathbf{x}_0) - P_{\text{in}}(\mathbf{x}_0)$ and realizing that the integral containing $\frac{\partial}{\partial z} P_{\text{in}}$ describes the reflected field from an ideal rigid infinite plane (denoted as $P_{\text{refl}}^{\text{rigid}}(\mathbf{x})$) yields

$$P_{\text{tot}}(\mathbf{x}) = P_{\text{in}}(\mathbf{x}) + P_{\text{refl}}^{\text{rigid}}(\mathbf{x}) - $$
$$- 2 \int_\Omega \frac{\partial}{\partial z} P_{\text{tot}}(\mathbf{x}_0) G(\mathbf{x}, \mathbf{x}_0) d\mathbf{x}_0 \tag{8}$$

The integral explicitly contains the three components of the total pressure field, as discussed in the foregoing.

Finally, the pressure gradient in the air can be expressed by the Euler's relation $\frac{\partial}{\partial z} P(\mathbf{x}) = -\rho_0 A(\mathbf{x})$, and the radiation problem can coupled with the surface by the boundary

condition (4). Restricting the receiver position to the elastic surface the above integral takes the form

$$P_{\text{tot}}(\mathbf{x}) = 2P_{\text{in}}(\mathbf{x}) +$$
$$+ 2\rho_0 \int_\Omega \left(\int_\Omega Y(\mathbf{x}_0, \mathbf{x}_1) P_{\text{tot}}(\mathbf{x}_1) \, d\mathbf{x}_1 \right) G(\mathbf{x}, \mathbf{x}_0) d\mathbf{x}_0,$$
(9)

describing the total field implicitly at an arbitrary receiver position on the horizontal plane $\mathbf{x} = [x,\ y,\ 0]^T \in \Omega$.

2.2. Numerical solution of the integral formula

Equation (9) presents the total pressure field as an integral equation which cannot be solved analytically. However, it can be numerically solved by discretizing the elastic surface into I elements, with the center of each element $\mathbf{x}_i$ and area $d\Omega_i$. The complex amplitudes of pressure and normal velocity at $\mathbf{x}_i$ are given by the vectors $\mathbf{p} = P_i = P(\mathbf{x}_i)$ and $\mathbf{a} = A_i = A(\mathbf{x}_i)$, and their interconnection is described by the admittance matrix

$$\mathbf{a} = A_i = \mathbf{Y}\mathbf{p} = \sum_{j=1}^I Y_{ij} P_j.$$
(10)

By introducing the Green's matrix on the surface

$$\mathbf{G} = G_{ij} = \int_{d\Omega_i} G(\mathbf{x}_j, \mathbf{x}_0) d\mathbf{x}_0, \quad \mathbf{x}_j = [x,\ y,\ z = 0]^T$$
(11)

and discretizing equation (9), we obtain

$$\mathbf{p}_{\text{tot}} = 2\mathbf{p}_{\text{in}} + 2\rho_0 \mathbf{G} \, \mathbf{Y} \, \mathbf{p}_{\text{tot}}.$$
(12)

The total field on the surface of the plate is obtained by solving the system of equations as

$$\mathbf{p}_{\text{tot}} = 2 \left(\mathbf{I} - 2\rho_0 \mathbf{G}\mathbf{Y} \right)^{-1} \mathbf{p}_{\text{in}},$$
(13)

and the corresponding normal velocity distribution from the discrete form of equation (4) as

$$\mathbf{v}_{\text{tot}} = \frac{1}{\mathrm{j}\omega} \mathbf{Y} \mathbf{p}_{\text{tot}}.$$
(14)

2.3. Numerical estimation of the admittance matrix

In the foregoing it was highlighted that once the admittance matrix of the elastic surface is known, scattering of an arbitrary incident wave can be modeled numerically. Now it is discussed how the admittance matrix can be obtained by measuring the pressure and the acceleration of the elastic surface.

By definition, the mutual admittance between receiver position $\mathbf{x}$ and source position $\mathbf{x}_0$ is given by the acceleration at the receiver position, assuming a spatial Dirac-delta pressure distribution at the source position, as given by (5). Again, by discretizing the surface into I elements, the discrete form of (5) is given by

$$Y_{ij} = A_i, \quad \text{if} \quad P_i = \delta_{ij},$$
(15)

where δ_{ij} denotes a Kronecker-delta at the j-th grid position. Hence, the j-th column of the admittance matrix is given by the surface acceleration vector due to a point-like pressure distribution, excited at the j-th element. Therefore, the direct measurement of the admittance matrix would require the measurement of the surface acceleration by ensuring Kronecker-delta pressure excitation over all the grid points.

Obviously, such a Dirac-like pressure distribution can not be physically realized with available pressure sources (e.g. a loudspeaker) due to the sound source radiation characteristics and the presence of the re-radiated sound field component. Still, the required pressure distribution can be numerically reproduced as the linear combination of a number of I independent measurements: Assume a matrix of pressure measurement results $\mathbf{P}$ with the size of $I \times I$. In the pressure matrix the j-th column represents the pressure distribution over the measurement grid for the j-th independent measurement. Simultaneously, the acceleration is also captured over the measurement grid in each measurement, resulting in the $I \times I$ sized acceleration matrix $\mathbf{A}$. Once the columns of the pressure matrix are linearly independent, a Kronecker-delta at an arbitrary grid position can be expressed as the linear combination of the matrix columns. With the required transform matrix denoted by $\mathbf{T}$, with the j-th column containing the required combination coefficients for expressing Kronecker-delta at the j-th position, the system of equation can be written in the matrix form of

$$\mathbf{P}\mathbf{T} = \mathbf{I}, \quad \rightarrow \quad \mathbf{T} = \mathbf{P}^{-1}$$
(16)

with $\mathbf{I}$ denoting the identity matrix. Performing the same linear transform on the measured acceleration matrix directly yields the required admittance matrix, i.e.

$$\mathbf{A}\mathbf{T} = \mathbf{A}\mathbf{P}^{-1} = \mathbf{Y}$$
(17)

holds. This equation is obviously the numerical form of (4) with I independent measurements.

As the central result of the present section, the admittance matrix can be estimated by performing a number of I measurements, acquiring both the surface pressure and acceleration at each grid positions. The independent measurements can be realized e.g. by exposing the planar surface to the sound field of a dynamic loudspeaker with a number of I different loudspeaker positions. In the following section the actual admittance measurement of a relatively small-sized porous absorber will be presented.

2.4. Definition of the absorption coefficient of extended reactive surfaces

Once the admittance matrix of an elastic surface is estimated, the total pressure field and velocity distribution on the surface of the absorber can be evaluated according to (13) and (14) for an arbitrary incident wave. These quantities allows for the prediction of the absorption characteristics of the surface. The incident field is assumed to be a plane wave arriving to the elastic surface at an elevation angle of θ and azimuth angle of ϕ, described by

$$P_{\text{in}}(\mathbf{x}, \theta, \phi) = e^{-\mathrm{j}k(\cos\phi\sin\theta x + \sin\phi\sin\theta y + \cos\theta z)}.$$
(18)

Intensity based absorption estimation:
As the most straightforward and physically correct estimation, the directional absorption coefficient of the elastic surface can be defined as (see eq. (12.30) [10])

$$\alpha(\theta, \phi) = \frac{\Pi_{\text{abs}}(\theta, \phi)}{\Pi_{\text{in}}(\theta)} =$$
$$= Z_0 \frac{\mathrm{Re}\left(\int_\Omega P_{\text{tot}}(\mathbf{x}, \theta, \phi) V_{\text{tot}}^*(\mathbf{x}, \theta, \phi) \, d\mathbf{x} \right)}{\cos\theta \, S_\Omega}, \quad (19)$$
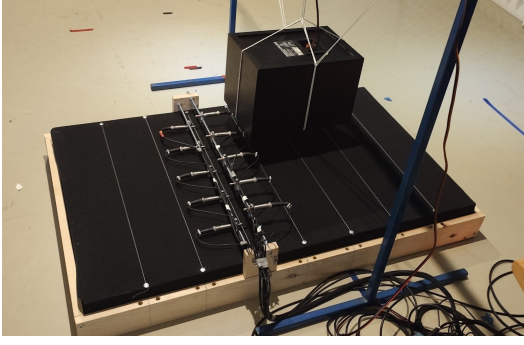
Figure 3: The result of TMM modeling

Figure 2: Porous absorber under investigation

with Π_{abs} and Π_{in} being the absorbed and incident power, S_Ω being the area of the elastic surface and $Z_0 = \rho_c c$ being the specific impedance of air.

The diffuse field absorption coefficient is calculated by averaging the absorbed and incident power over the possible directions of incidence, resulting in

$$\alpha^{\text{diff}} = \frac{\int_0^{2\pi} \int_0^{\pi/2} \Pi_{\text{abs}}(\theta, \phi) \sin\theta \mathrm{d}\theta \, \mathrm{d}\phi}{\int_0^{2\pi} \int_0^{\pi/2} \Pi_{\text{in}}(\theta) \sin\theta \mathrm{d}\theta \, \mathrm{d}\phi} =$$
$$= Z_0 \frac{\int_0^{2\pi} \int_0^{\pi/2} \Pi_{\text{abs}}(\theta, \phi) \sin\theta \mathrm{d}\theta \, \mathrm{d}\phi}{\pi S_\Omega}. \quad (20)$$

Locally reactive approximations:

Along with the strict mathematical definition, a simplified approach is also investigated in the following, introduced by Thomasson [4]. The model under discussion assumes a homogeneous, locally reactive impedance over the surface of the absorber given by Z_A, but includes size effects, by evaluating (19) analytically. The resulting directional absorption coefficient is given by

$$\alpha(\theta, \phi) = \frac{1}{\cos\theta} \frac{4\text{Re}Z_A}{|Z_A + Z_R|^2}, \quad (21)$$

where the locally reacting surface impedance can be calculated as

$$Z_A = \frac{1}{Z_0} \frac{\int_\Omega P_{\text{total}}(\mathbf{x}) \mathrm{d}\mathbf{x}}{\int_\Omega V_{\text{total}}(\mathbf{x}) \mathrm{d}\mathbf{x}}, \quad (22)$$

and Z_R is the normalized radiation impedance of the surface, calculated numerically as proposed in Appendix 12.A in [10]. Finally, as the roughest approximation, in the limiting case when the absorber surface is assumed to be infinite with homogeneous surface impedance of Z_A (calculated from (22)), and with the radiation impedance being $Z_R = 1/\cos\theta$, the classic absorption formula is recovered

$$\alpha_\infty(\theta) = \frac{4\text{Re}Z_A \cos\theta}{|Z_A \cos\theta + 1|^2}. \quad (23)$$

In the following these absorption formulae are evaluated for both an analytical absorber model and for an actual porous absorber, in order to compare the fully physical solution (19) and (20) with the above locally reactive approximations.
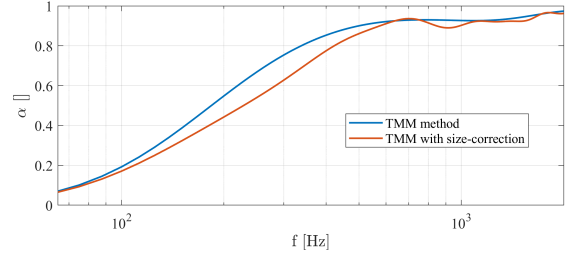
3. In-situ measurement of the admittance matrix

3.1. Porous absorber under investigation

The porous absorber under investigation is depicted in Figure 2. The absorber is the single sheet of rockwool, with plywood framing and backing, both considered to be ideally rigid in the following. The dimensions of the sample were $L_x = 0.6\,\text{m}$, $L_y = 1\,\text{m}$, $L_z = 0.1\,\text{m}$, meaning a total surface of $S_\Omega = 0.6\,\text{m}^2$, being of relatively small-size compared standard impedance measurement requirements. The type of the absorber is Airrock ND (normal density), with the rated flow resistivity of $\sigma = 12\,000\,\text{Pas/m}^2$ according to the manufacturer's data sheet.

As the most simple absorption estimation, the single porous layer was modeled with the 1-dimensional transfer matrix method (TMM) as described in [10], by employing an equivalent fluid model for the porous material using the Mechel-Grundmann model [11]. The result of the prediction is depicted in Figure 3 in case of assuming a single layer of infinite dimensions, and by taking the finite size into account by using a simple radiation efficiency-based correction term [10]. In both cases normal incidence absorption is illustrated.

As a more accurate reference, in the current geometry (i.e. a rectangular layer of fluid with rigid boundary conditions) the surface admittance matrix can be expressed analytically as a modal superposition, reading [12]

$$Y_{\text{an}}(\mathbf{x}, \mathbf{x}_0) = -\frac{1}{\rho_0} \sum_{\mathbf{m}} \Phi_{\mathbf{m}}(\mathbf{x}) \Phi_{\mathbf{m}}(\mathbf{x}_0) \frac{k_z^{\mathbf{m}}}{\cot(k_z^{\mathbf{m}} L_z)}. \quad (24)$$

In the expression $\Phi_{\mathbf{m}}(\mathbf{x}) = \Phi_m(x) \cdot \Phi_n(y)$ are the set of orthogonal modal basis functions, in the current geometry given by

$$\Phi_m(x) = \begin{cases} \dfrac{1}{\sqrt{L_x}}, & m = 0 \\ \sqrt{\dfrac{2}{L_x}} \cos\dfrac{m\pi}{L_x}x, & m > 0 \end{cases} \quad (25)$$

$$\Phi_n(y) = \begin{cases} \dfrac{1}{\sqrt{L_y}}, & n = 0 \\ \sqrt{\dfrac{2}{L_y}} \cos\dfrac{m\pi}{L_y}y, & n > 0 \end{cases} \quad (26)$$

and where $k_z^{\mathbf{m}}$ is defined as

$$k_z^{\mathbf{m}} = \sqrt{\left(\frac{\omega}{c_{\text{fl}}}\right)^2 - \left(\frac{m\pi}{L_x}\right)^2 - \left(\frac{n\pi}{L_y}\right)^2}. \quad (27)$$

Here c_{fl} denotes the speed of sound in the equivalent fluid modeling the porous material, obtained from the Mechel-Grundmann model, with the flow resistivity chosen to $\sigma = 12\,000\,\text{Pas/m}^2$ in correspondence with the manufacturer's data sheet.

From the analytical admittance matrix the total pressure and velocity can be calculated on the absorber surface according to (13)
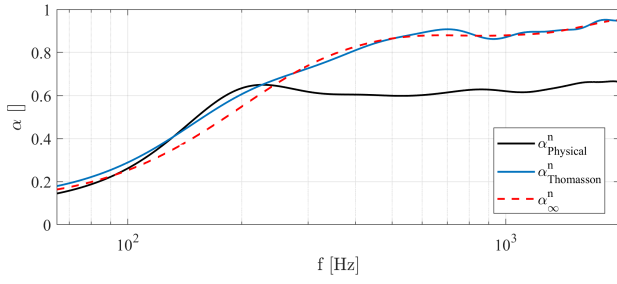
Figure 4: Estimated normal absorption coefficient of the porous absorber, by applying the analytical model for the admittance matrix estimation.

Figure 5: Measurement setup for validating the analytical and numerical results.

and (14) in case of an incident plane wave, allowing the estimation of the absorption coefficient. Figure 4 depicts the estimated normal absorption coefficient of the analytical model, by evaluating the proposed physical based absorption coefficient (19), and the locally reactive approximations: the Thomasson model (21) and using the classic absorption formula (23), the latter omitting finite-size correction. It is revealed that the locally reactive, homogeneous approximations give qualitatively similar results, both reflecting that above a certain frequency ($\approx 400\,\mathrm{Hz}$) the porous layer completely absorbs the incident sound energy, with an absorption coefficient close to unity. On the other hand, the full physical solution reflects a decreased absorption even at higher frequencies, with the maximal absorption coefficient being around 0.6.

3.2. Measurement of the admittance matrix

In Section 2.3, the process of estimating the admittance matrix was discussed. This estimation involves simultaneous measurements of normal surface acceleration and surface pressure over a predefined grid on the surface. The grid contains I grid points, with I different loudspeaker positions. The actual grid used in practice was a 5×7 equidistant arrangement, excluding boundary points, resulting in spatial sampling distances of $\Delta x = 0.1\,\mathrm{m}$ and $\Delta y = 0.125\,\mathrm{m}$.

To measure particle acceleration, a two-microphone method was employed in an anechoic chamber, as shown in Figure 5. At each measurement position, two vertically shifted microphone pairs recorded local pressure signals. The vertical acceleration was then estimated from the microphone signals using the following equation:

$$A(\mathbf{x}) \approx -\frac{1}{\rho_0}\frac{P_u(\mathbf{x}) - P_l(\mathbf{x})}{\Delta z}, \qquad (28)$$

where P_u and P_l denote the pressure signals of the upper and lower microphones, respectively, and Δz is the microphone spacing.

The microphone spacing plays a significant role in determining the frequency range for reliable measurements. A small microphone distance is necessary for accurate measurements at higher frequencies, while a larger distance is needed to avoid the severe effect of phase errors at lower frequencies. To cover a wide frequency range, two independent measurements were conducted with microphone spacings of $\Delta z = 4\,\mathrm{cm}$ and $\Delta z = 12\,\mathrm{cm}$. The results were then combined using a Hann window between 300 and 500 Hz. This setup allowed feasible acceleration measurement up to approximately $2\,\mathrm{kHz}$ and an experimental lower frequency limit of around $70\,\mathrm{Hz}$ [13]. To reduce the number of measurements, both acceleration and pressure were measured si-
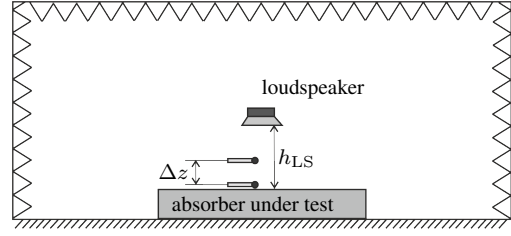
multaneously in five different positions, as depicted in Figure 2 (a).

For improved measurement results, the frequency transfer of individual microphone pairs was equalized using the microphone switching technique [14]. Additionally, the microphone spacing was adjusted by comparing the results of acceleration approximation with direct measurements using a Microflown sensor.

The choice of loudspeaker height, denoted as h_{LS} in Figure 5, is crucial for processing the measurement data. For the measured pressure matrix in Equation (17) to be invertible, all the measurements must be linearly independent. This means that the Kronecker-delta must be available as a linear combination of the pressure records over the surface. To ensure this, in each loudspeaker position, either the amplitude or the phase of the incident sound field must change significantly along the spatial extension of the absorber. To meet this requirement, the loudspeaker was placed above an individual grid point as close as possible during each measurement, resulting in loudspeaker heights of $h_{\mathrm{LS}} = 6\,\mathrm{cm}$ and $h_{\mathrm{LS}} = 20\,\mathrm{cm}$ for the consecutive measurements.

3.3. Measurement based absorption charateristics estimation

Having measured the admittance matrix of the absorbing surface by the extended two-microphone measurement technique, the surface pressure and velocity can be evaulated (see (13) and (14)) for an arbitrary incident field, from which the absorption characteristics can be predicted.

Again, both physically motivated intensity based (extendedly reactive) absorption and locally reactive approximations were investigated by evaluating (19) and (20) for the former and (21) and (23) for the latter. The results are illustrated in Figure 6.

Figure 6 (a) depicts the normal incident absorption coefficient as the function of frequency, allowing comparison of the extendedly reactive and locally reactive models. The obtained absorption characteristics qualitatively matched well with the analytical model shown in Figure 4. However, the locally reactive model tended to overestimate the absorption coefficient at higher frequencies (above approximately 300 Hz). Additionally, the non-locally reactive approach showed a pronounced peak in the absorption coefficient around 180 Hz, which was also evident in Thomasson's size-corrected locally reactive approximation but suppressed in the infinite local reactive surface approximation. These significant discrepancies between the extendedly and locally reactive models supports the validity of the extendedly reactive modeling over the locally reactive approximation, despite the substantial number of required measurements. Further investigation into the physical mechanisms responsible for these observations is planned for future research.

In case of intensity based absorption both normal and oblique incident absorption coefficients are depicted in Figure 6 (b) along
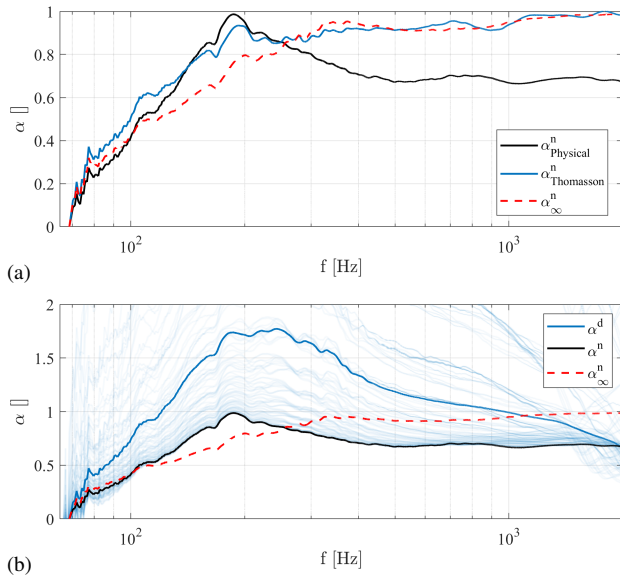
Figure 6: Estimated normal incidence absorption coefficients comparing extended reactive and locally reactive models (a) and diffuse absorption characteristics from extendedly reactive estimation (b). Faded lines denote the individual directional absorption characteristics for different angles of incidence.

with the corresponding diffuse field absorption coefficient, by evaluating (20). It is important to note that lateral waves are absorbed with an absorption factor exceeding unity in the low-frequency range. This phenomenon can be attributed to diffraction effects at the edges of the absorber, where lateral waves tend to diffract towards the absorber material at low frequencies. Due to the decrease in incident power with increasing angle of incidence, the apparent absorbing coefficient increases with the angle of incidence in the frequency range where edge diffraction is significant.

4. Summary and conclusions

The current study focused on the modeling and measurement of planar porous absorbers. The mathematical model employed allowed for solving the acoustic scattering problem with arbitrary incident fields, enabling estimation of the acoustic absorption characteristics of the absorber surface.

The absorber's acoustic behavior was described using its a-priori known admittance matrix. Consequently, obtaining an accurate numerical estimation of the admittance matrix was crucial for a physically correct modeling of the absorbing surface. The paper introduced an extended two-microphone measurement technique to estimate the admittance matrix for an actual porous absorber layer made of a single sheet of rockwool. This technique involved a high number of individual measurements, determined by the square of the predefined measurement positions. By using the measured admittance matrix, the absorption characteristics of the rockwool layer were investigated and compared with results obtained from an analytical model, showing good agreement between theoretical and measured outcomes.

It was observed that for the small-sized absorber sample in this study, significant discrepancies emerged between the introduced extendedly reactive model and traditional locally reactive approximations. However, the detailed analysis of the underlying physical processes responsible for the observed absorption characteris-

tics exceeded the scope of the present work and is suggested as a topic for future research.

Last but not least, the validation of the present modeling and measurement method poses difficulties, as the absorption characteristics of a single absorber sheet cannot be directly compared to the results of standardized measurement methods. A possible validation method for the foregoing could involve comparing the sound field above the absorber surface with actual microphone measurement data using a suitably chosen, physically realizable incident wave field. Elaborating on this verification method is once again the topic of further research.

5. Acknowledgment

References

[1] ISO 354:2003. Standard, International Organization for Standardization, Geneva, CH, 2003.

[2] ISO 10534-2:1998. Standard, International Organization for Standardization, Geneva, CH, 1998.

[3] E. Brandao, A. Lenzi, , and S. Paul. A review on in situ impedance andsound absorption measurement techniques. *Acta Acoustica United with Acoustica*, 101:443–463, 2015.

[4] S.-I. Thomasson. On the absorption coefficient. *Acta Acoustica United with Acoustica*, 44(4):265–273, 1980.

[5] S.-I. Thomasson. Theory and experiments on the sound absorption as function of the area. Technical Report TRITA-TAK-8201, KTH Stockholm, 1982.

[6] Heinrich Kuttruff. *Room Acoustics*. CRC Press, 2017.

[7] G. Firtha and Cs. Huszty. Measurement based absorption characteristics estimation of extended reactive surfaces. In *Forum Acusticum 2023*, Turin, Italy, September 2023.

[8] P. M. Morse and K. U. Ingard. *Theoretical Acoustics*. McGraw-Hill Book Company, New York, NY, 1st edition, 1968.

[9] E. G. Williams. *Fourier Acoustics: Sound Radiation and Nearfield Acoustical Holography*. Academic Press, London, 1st edition, 1999.

[10] Jean Allard and Noureddine Atalla. *Propagation of Sound in Porous Media: Modelling Sound Absorbing Materials*. Wiley, 2009.

[11] F. P. Mechel. *Formulas of Acoustics*. Springer, 2002.

[12] G. Firtha and Cs. Huszty. A 3d modeling method of layered acoustic material structures with finite dimensions. In *Internoise2023*, Tokyo, China, August 2023.

[13] Y. Champoux and A. L'Espérance. Numerical evaluation of errors associated with the measurement of acoustic impedance in a free field using two microphones and aspectrum analyzer. *J. Acoust. Soc. Am.*

[14] J. Chung and D. Blaser. Transfer function method of measuring in-duct acoustic properties. ii. experiment. *J. Acoust. Soc. Am.*, (68):914–921, 1980.